Pergamon

*Journal of Structural Geology*, Vol. 18, Nos 2/3, pp. 155 to 167, 1996

0191-8141/96 $15.00 + 0.00

0191-8141(96)00122-0

# Fault population description and prediction using examples from the offshore U.K.

TIM NEEDHAM and GRAHAM YIELDING

Badley Earth Sciences Limited, North Beck House, North Beck Lane, Hundleby, Spilsby, Lincolnshire PE23 5NB, U.K.

and

RICHARD FOX

BP International Limited, Sunbury Research Centre, Chertsey Road, Sunbury-on-Thames, Middlesex TW16 7LN, U.K.

(*Received* 9 *December* 1994; *accepted in revised form* 22 *September* 1995)

**Abstract**—Three-dimensional seismic interpretation and well-core data were analysed to characterize the fault populations in two offshore U.K. hydrocarbon fields. Comparison of multiline fault-throw samples from seismic-scale faults with displacement samples, measured on well-core fractures, shows that the displacement population is described by a power law. Faults seen in core and on seismic data are consistent with one another and appear to belong to the same continuous population; therefore the number of intermediate-scale faults can be predicted. Fault lengths are much more difficult to measure due to resolution effects and the size of the sampling area. Fault linkage also introduces some problems, as it may prove difficult to determine which splay should be included in the length measurement when faults branch. Well-core fault and fracture sets have been analysed in terms of their spacing, which also appears to be described by a power law and is clearly distinguishable from regular spacing. Comparison of core-scale fracture orientations with seismically-mapped faults shows that the two have similar azimuth distributions. Subsurface data, either well core or seismic, is particularly amenable to analysis by one-dimensional sampling.

## INTRODUCTION

Predicting the number of small-scale faults has important applications in the successful management of hydrocarbon reservoirs. Small-scale faults have significant effects on the flow of fluids in the subsurface, most often acting as barriers due to the cataclastic reduction of porosity and permeability in the fault zone (Antonellini & Aydin 1994). Even small-displacement faults are important as they may have throws that are sufficiently large to offset individual reservoir zones within a producing succession, resulting in a reduction in reservoir connectivity. Larger faults are well known to act as seals between different compartments in a hydrocarbon field or to act as a seal for the entire accumulation (Smith 1966, Watts 1987). It is important, therefore, to be able to estimate the likely characteristics of the fault population within an oil or gas field. The fault population at the seismic and sub-sesimic scales can be characterized in terms of length, displacement, spacing and orientation. Characterization of the fault population can also be used to estimate the relative contributions of seismic and sub-seismic scale faults to the strain in extensional basins (Walsh *et al.* 1991, Marrett & Allmendinger 1992).

Prediction of the fault population below the scale of seismic resolution is believed to be feasible because many aspects of faults are fractal. That is, faults tend to be self-similar over a wide range of scales, so that the proportion of larger and smaller features remains the same. Such populations are described by a power-law frequency distribution of the form:

$$N = aS^{-\mathcal{D}} \tag{1}$$

where $N$ is the number of features having a size greater than or equal to $S$ (e.g. fault displacement or fault length). A graph of $N$ against $S$ on logarithmic axes is a straight line with slope $-\mathcal{D}$ ($\mathcal{D}$ is termed the fractal dimension). Therefore if the population distribution can be defined at the scale of seismic reflection observations, it can be extrapolated to sub-seismic scales to allow the prediction of the number of small faults. This prediction can be further constrained by the use of core fracture data that should fall on or near the projected slope of the seismically-resolved fault population. Constraint of the population slope by fractures showing offsets in the order of 1–100 mm allows a better prediction of faults at scales intermediate between core and seismic observation (Childs *et al.* 1990). Estimating the number of these faults allows modelling to be undertaken to gauge the sensitivity of reservoir performance to small-scale faulting (Sassi *et al.* 1992, Gauthier & Lake 1993, Munthe *et al.* 1993, Heath *et al.* 1994).

An understanding of the dimension of the sampling

domain is important for the practical application of the results. A volume of faulted rock could be sampled in three dimensions by counting all the fault surfaces in that volume. A two-dimensional sample would be obtained by counting all the fault traces on a particular horizon within that volume. Similarly, a one-dimensional sample would be obtained by counting fault cuts on one horizon on a cross-section or one line drawn across a map view. A multiline one-dimensional sample can be obtained by counting fault cuts on one horizon on a series of cross-sections or many parallel lines on the same map. Subsurface data is particularly amenable to multiline sampling as seismic lines provide a series of regularly spaced, parallel, sample lines. The multiline sample does not resemble a two-dimensional sample. In a two-dimensional sample each fault trace provides only one measurement (e.g. of fault-trace length or maximum displacement), whereas in a multiline sample each fault will provide a measurement on every sample line that crosses it. These different sample types provide differing ways of characterizing the fault population and are geometrically related to one another (Heffer & Bevan 1990, Marrett & Allmendinger 1991, Yielding *et al.* 1992, 1996, Walsh *et al.* 1994).

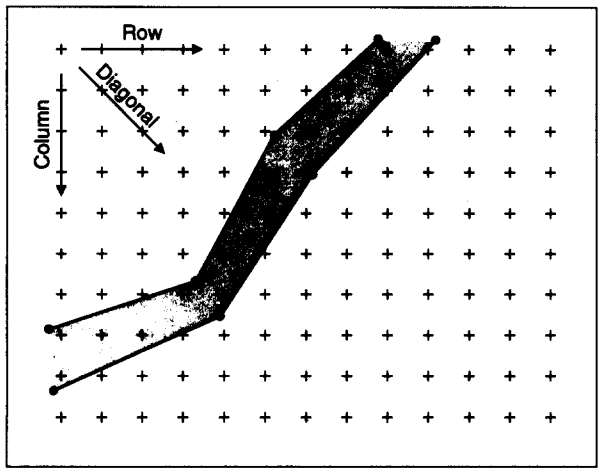


Fig. 1. Map showing sampling of horizon data held in grid form. The data consist of a regularly spaced grid, each node having a two-way time or depth value. The fault (shaded) is represented as a polygonal outline corresponding to its hangingwall and footwall cut-offs. Sampling can take place along grid rows, down columns or diagonally. Pairs of grid nodes on opposite sides of the fault are compared to find the difference in elevation and, hence, the throw on the fault. Local fault orientations can also be calculated between adjacent nodes on the fault polygon.

## SAMPLING FAULT POPULATIONS FROM SUBSURFACE DATA

There are two main sources of subsurface data that can be used in fault population analysis. One is commercial seismic reflection data and the other is well core. Many producing hydrocarbon fields have now been imaged by three-dimensional reflection seismic surveys where lines are acquired at a line spacing of 50 m or less. Such surveys essentially provide a continuous volume of data allowing the interpretation of reflective horizons as continuous surfaces. This supersedes two-dimensional seismic reflection surveys that have much greater line spacings. Continuous horizon interpretations of three-dimensional seismic data sets can be achieved by auto-tracking, the automated interpretation of a given reflector, throughout the entire data volume. Once this continuous interpretation has been achieved, the interpreted horizon may be viewed in map form using specific attributes, such as the magnitude of dip or the azimuth of that dip, to highlight structural detail (Dalley *et al.* 1989). Use of attributes such as dip and azimuth allows the identification of many small faults that would not be interpreted by performing only a conventional interpretation of vertical seismic sections.

Not all horizons are continuously interpreted using auto-tracking, particularly in areas of poorer reflection character (i.e. low signal to noise ratio). A three-dimensional seismic data set may be interpreted on every fourth or fifth line, but this still gives excellent coverage for multiline sampling. Such an interpretation is, however, processed during mapping and depth conversion into an $x$, $y$ grid of regularly spaced nodes, each of which has a $z$-value for the depth or two-way-travel time (TWT) to the horizon at that point. Faults are represented by polygonal outlines, corresponding to the footwall and hangingwall cut-offs on that horizon (Fig. 1). It is still possible to sample an interpretation held in this gridded form. The depth or TWT to pairs of nodes on the opposite side of a fault can be used to calculate the throw on that fault (Fig. 1). Sampling can take place along rows, down columns or diagonally across the grid nodes to generate a multiline sample. The sampling direction would be selected on the basis of the dominant fault orientation; the optimum sampling direction is perpendicular to the main fault trend. This procedure has been followed for the analysis described here. Depth grids are desirable as they allow direct comparison with data obtained from well cores.

Well core provides information on the fault population below the scale of seismic resolution. Modern coring techniques allow long runs of core to be taken with very good recovery rates. It is not uncommon, in the North Sea, for entire reservoir successions to be cored. This gives long sample lines from which fracture density, displacement, spacing and orientation data can be obtained. As seismic mapping tends to concentrate on defining the structure of the top of a hydrocarbon reservoir, and coring aims to sample the reservoir itself, the two data sources are comparable. Direct observation of the reservoir fault population allows an assessment to be made of the likely effects of these faults on fluid flow.

Here, we describe the application of fault population analysis for two offshore U.K. fields, A and B. The objective of these studies is to characterize the fault population so that the results might be used in reservoir flow simulations and predictions made about the likely fault density along the proposed trajectory of a horizontal well. Both fields had three-dimensional seismic sur-

veys over them and well core for characterizing the sub-seismic fault population.

## FAULT POPULATION ANALYSIS, FIELD A

Field A is developed in a Palaeozoic, predominantly fluvial, red-bed sequence. The area has undergone at least two phases of Mesozoic extension. Two seismically-mapped horizons were used in the analysis. Top Reservoir and Intra-reservoir. Top Reservoir is a good seismic reflector but Intra-reservoir is not as good. The fault pattern at the top reservoir horizon is shown in Fig. 2. The horizon maps were available in grid form with digitized fault polygons. The grid is oriented parallel to the seismic survey and not in N–S rows and E–W columns. Although large faults are present within the data area, regional seismic mapping shows that larger faults, not represented in this data set, exist adjacent to Field A. Displacement data were measured perpendicular to the dominant fault orientation. Fault lengths were also measured from the maps of each horizon.

Sub-seismic scale fault data were obtained from core from five wells. Cores showed the field to be highly faulted at the sub-seismic scale. Fracture types included open fractures, cataclastic granulation seams, partially cemented and cemented fractures. Larger fault zones were also encountered. A total of 2103 m of core, containing *ca* 5400 fractures, was included in the analysis. The longest core is 717 m, the shortest has a length of 158 m. Fault displacements and orientations were measured for one of the well cores, the others provided fault density data only. The total number of fractures cutting the centreline of the slabbed face of each core was recorded. This was then divided by the length of the core to obtain the cumulative fault density per m of core. Fault density values for Field A range from 0.65 to 1.80 $m^{-1}$.

### *One-dimensional sampling of displacements*

Multiline sampling techniques were used to characterize the seismic-scale fault population. The direction of sampling was approximately perpendicular to the dominant strike direction of faults within the field. Figure 3 shows logarithmic cumulative frequency plots for fault throws sampled from the Top Reservoir and Intra-reservoir horizons. These curves have three segments (Walsh *et al.* 1994):

(i) a subhorizontal left-hand segment indicating a lack of observations below the limit of seismic resolution. This effect is termed left-hand truncation (see Pickering *et al.* 1995);

(ii) a moderately-dipping central segment whose linear nature indicates a power-law relationship between fault throw and cumulative number;

(iii) a steeply dipping right-hand segment, created by the multiline sampling method and not representative of the fault population.

The central segment, which provides information about the actual fault population, is well enough developed in each case to allow the slope for the data sets to be calculated. These are −0.84 for the Top Reservoir and −0.95 for the Intra-reservoir horizon.

The measured displacements from well core are also plotted as a logarithmic cumulative frequency plot (Fig. 4a). The data plot as a straight line extending over one order of magnitude. Undersampling at the low-displacement end, below 8 mm, results in a decrease in the slope of that portion of the curve. The slope increases at displacements greater than 100 mm because these are undersampled due to the finite size of the core.

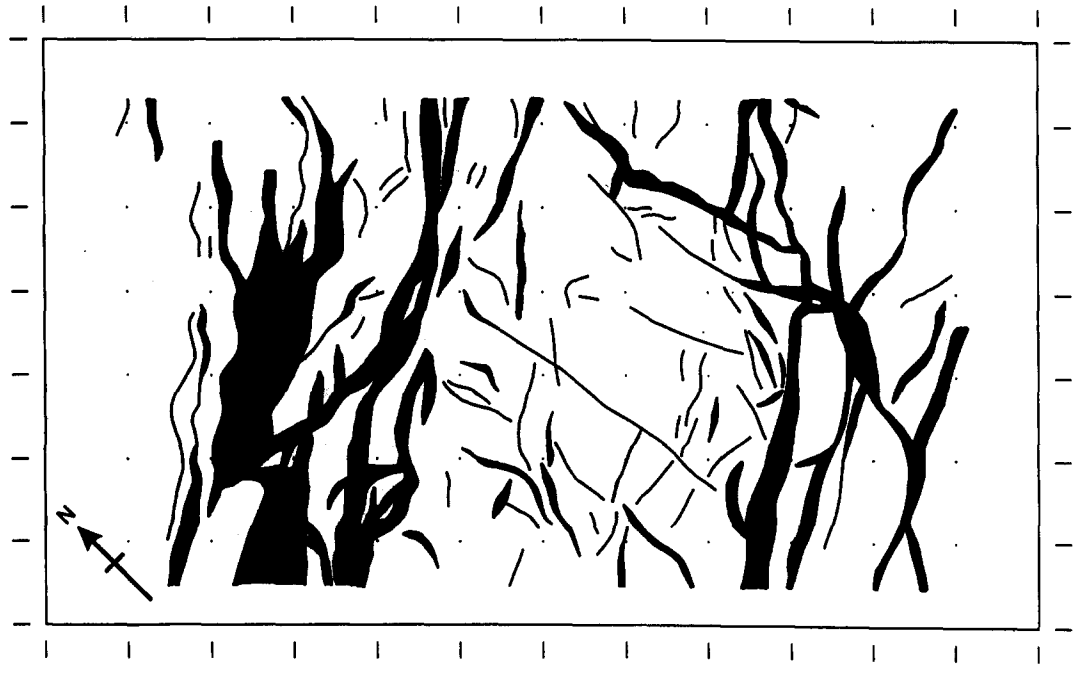


Fig. 2. Map of fault pattern at the Top Reservoir horizon, Field A. The fault heave polygons are shown in black. Note that the seismic survey co-ordinate reference frame is used. Ticks at the grid margin have a 1 km spacing.

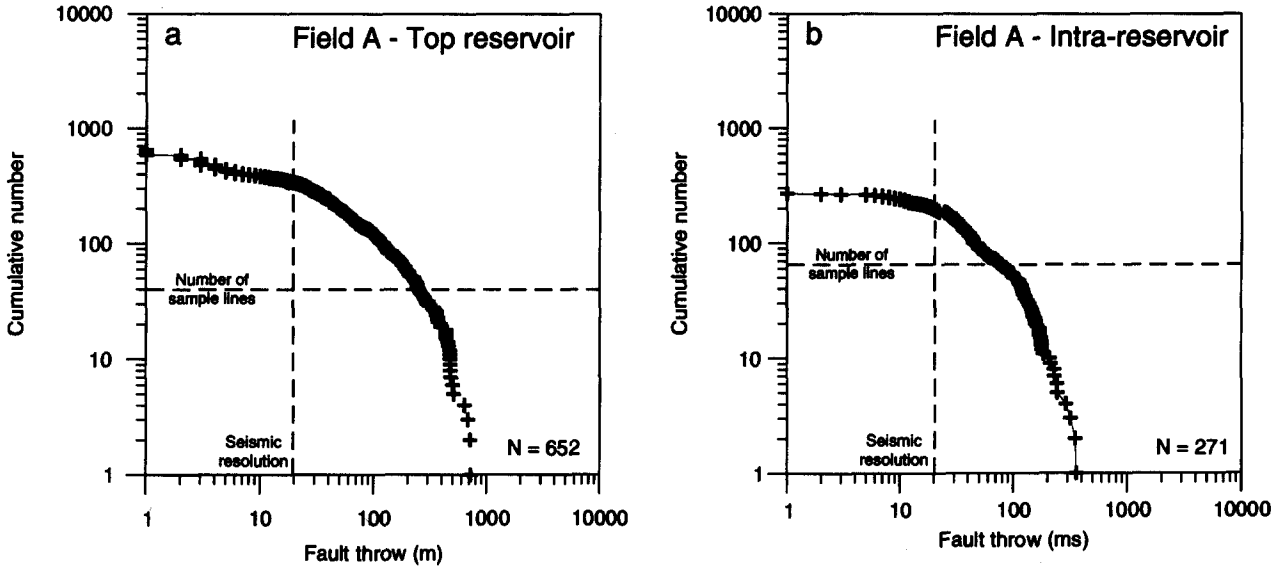


Fig. 3. Multiline one-dimensional samples of fault throw from (a) Top Reservoir and (b) Intra-reservoir horizons. Each displays the characteristic three-segment form of multiline samples. The Top Reservoir sample comprises fault cuts on 40 sample lines, total length 438 km; that from the Intra-reservoir horizon is from 64 sample lines, total length 167 km. Note that the Top Reservoir sample is in depth and the Intra-reservoir sample is in two-way time.

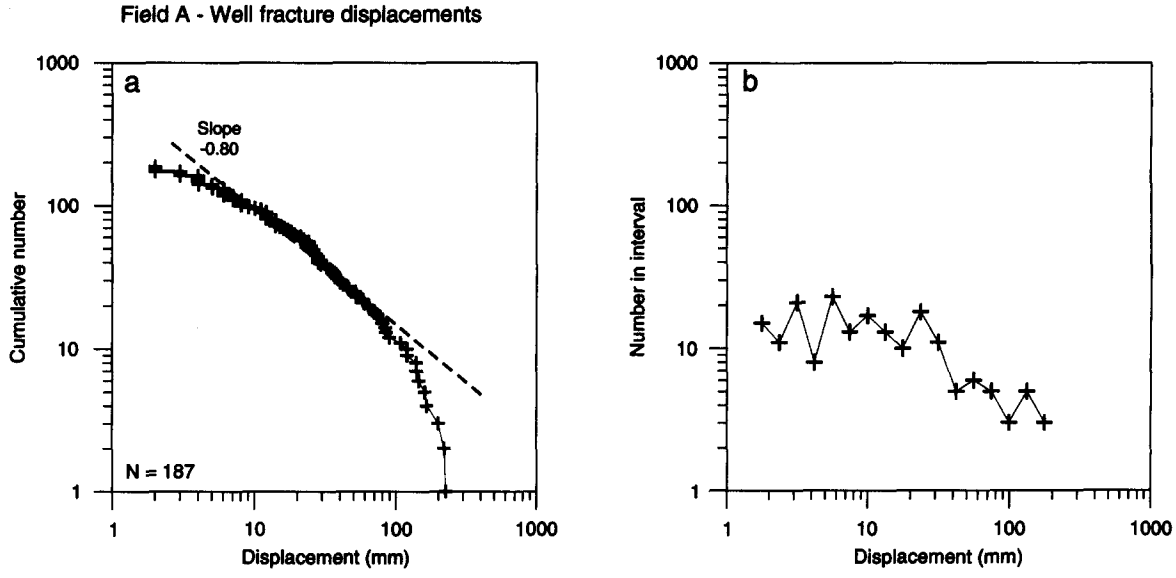


Fig. 4. (a) Cumulative frequency plot of fracture displacements from a Field A well. The curve shows a slightly convex-upwards form due to sampling effects at the upper and lower displacement ends. (b) Log-interval plot of the same data.

To assess sampling effects the log-interval method described by Pickering *et al.* (1995) has been used. This allows gaps in the data to be recognized. The method requires that data is binned into intervals of equal size on a log scale. The number of data points within each interval is then plotted on a log scale. An ideal data set (synthetic or completely-sampled natural) plots as a straight line of slope $-\mathfrak{D}$ with a slight fall-off at the right- and left-hand sides. The slope $-\mathfrak{D}$ is identical with that which would be measured on a log–log cumulative frequency graph. More irregular curves suggest that data gaps occur. The log-interval plot for the Field A core displacements (Fig. 4b) has an irregular form even in the central section of the curve. This suggests that not all intervals provide a fully representative data set. These sampling effects for well cores are discussed in more detail below in relation to the results from Field B where a larger data set was available and some of the effects are more pronounced.

To test whether these slopes can be used to predict, by extrapolation, the fault density at sub-seismic scales, the seismic scale results must be compared with the core data. First, the data must be normalized to cumulative fault density per km of sample line. Second, the fault density information from core must be corrected to account for differences in sample line orientation. The seismic data are from essentially horizontal sample lines whereas the core data are derived from vertical wells. The degree to which the fault population is sampled depends on the orientation of the sample line relative to

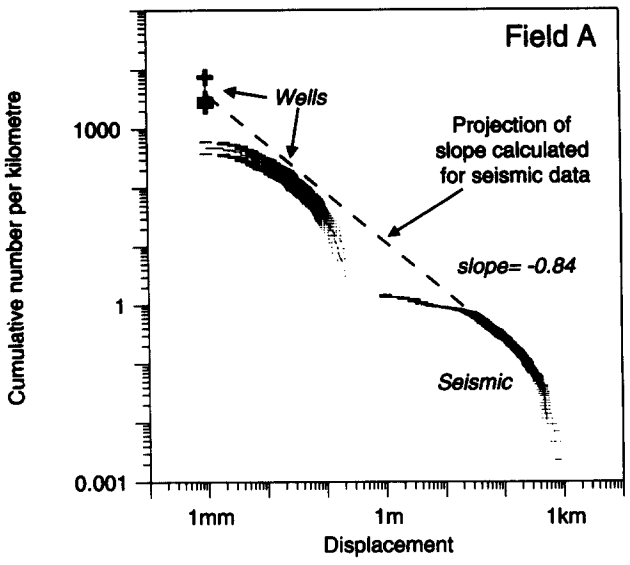


Fig. 5. Comparison of Top Reservoir seismic-scale throw data with well displacement data, for Field A. The slope of −0.84 was calculated for the seismic data (Fig. 3a) and is projected to lower displacement values. The well cumulative frequency curve is from Fig. 4. Wells with no measured displacement values have an assumed 1 mm lower threshold and are plotted in terms of total cumulative fault density per kilometre. The seismic-scale faults and well-core fractures appear to form part of the same population.

the dip of the faults being sampled. For instance, a vertical sample line such as a well would not encounter any vertical faults. Faults dipping at 45° would be equally sampled by both horizontal and vertical sample lines. In general, the sampled fault densities will differ by a factor of tan $\theta$, where $\theta$ is the fault dip. An average dip of 60° is appropriate for Field A. Figure 5 shows the comparison of well and seismic data for the Top Reservoir horizon. Measured well displacements are plotted as a cumulative frequency curve. For the wells with no displacement data, a threshold value of 1 mm has been assumed, i.e. every fracture detected in the well core is assumed to have a displacement of at least 1 mm. The cumulative fault density value (per km) is then plotted as a single point for each well. There is some variability from well to well but all lie within one order of magnitude of cumulative fault density. Well-core data represent a very local sample and previous studies have shown that fault density can vary from area to area within a field (Walsh *et al.* 1994). The variability of well-core results is therefore to be expected.

The slope of −0.84, calculated for the central segment of the Top Reservoir seismic data set, has been extrapolated to sub-seismic scales. It can be seen that the predicted fault densities are similar to those observed in the well cores. The measured core-displacement curve lies slightly below the projected slope due to the fact that only 10% of the fractures yielded a displacement value. The fault displacement observed at both seismic and core scales appear to form part of the same population. Using the simple power-law relationship (equation 1), a prediction of the density of fault cuts of various displacements can be made. The number of faults in any order-of-magnitude class (e.g. 1–10 m throw) likely to be encountered in a 1 km transect can also be predicted (Table 1). For faults in the 1–10 m throw range, i.e. those not sampled by core or seismic, it is predicted that a horizontal transect will encounter 11.1 fault cuts km$^{-1}$.

### *Fault lengths*

Two-dimensional sampling involves the measurement of fault attributes on a two-dimensional surface, generally an horizon map. Fault traces can be characterized either by their length or their maximum displacement. These two attributes should show a relationship as longer faults tend to have larger displacements. Trace lengths were sampled by making measurements from the Top Reservoir and Intra-reservoir horizon maps. Defining fault lengths can be difficult as faults tend to branch and link (e.g. see Fig. 2). The exact definition of what is a single fault or which splay should be followed in measuring length can be quite subjective. Factors such as continuity of strike and regularity of displacement pattern have to be considered when measuring fault lengths.

A further problem associated with two-dimensional sampling concerns edge effects or censoring bias. Whereas one-dimensional displacement sampling is objective in that each offset measured contributes a data point, in a two-dimensional sample not all fault traces give a true measurement of length because the size of the sample window is finite. Some fault traces extend outside the survey area and so give only a minimum estimate of fault length. This effect, the Type-A censoring of Pickering *et al.* (1995) is more important for very large faults that, by their very nature, cannot be entirely contained within the sample area. However, censoring affects faults of all sizes (see Fig. 2), and it is better to include all the 'part-faults' in the sample area (see Yielding *et al.* 1996).

Seismic resolution also has an important influence on the definition of fault trace lengths. A seismically-

Table 1. Prediction of sub-seismic fault density for Field A. The second column ('Cumulative fault density') indicates the number of fault cuts greater than or equal to the specified throw per 1 km of horizontal transect. These values are calculated using $N = 13d^{-0.84}$, which is the equation of the dashed line on Fig. 5. The third column ('Fault density per class') indicates the number of fault cuts within each logarithmic class per 1 km of horizontal transect; these values are simply the differences of successive numbers in column 2. For example, the power-law relationship predicts that there are 13 fault cuts per km having throw greater than or equal to 1 m, and 11.1 fault cuts per km having throw in the range 1–10 m

| Throw (m) | Cumulative fault density (km$^{-1}$) | Fault density per class (km$^{-1}$) |
|---|---|---|
| 100 | 0.27 | |
| | | 1.63 |
| 10 | 1.9 | |
| | | 11.1 |
| 1 | 13 | |
| | | 77 |
| 0.1 | 90 | |
| | | 532 |
| 0.01 | 622 | |
| | | 3683 |
| 0.001 | 4305 | |

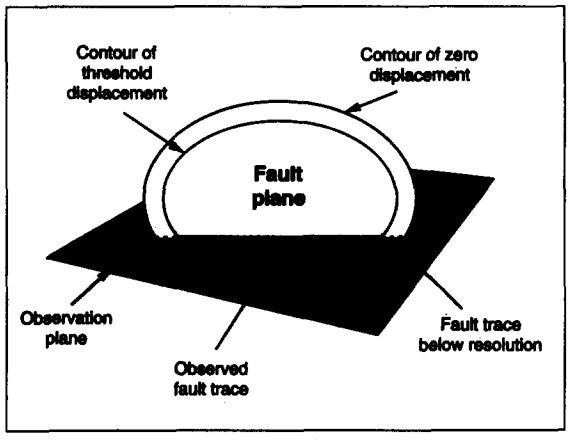


Fig. 6. Diagram, after Heffer & Bevan (1990), to illustrate why fault trace lengths observed on seismic interpretations are always shorter than the true length of the fault. The effect becomes proportionally greater for small faults.

imaged fault will appear shorter than its true length. This is because displacements near the tips of faults are below the limit of seismic resolution (Fig. 6). The difference between imaged length and true length is proportionally greater for small faults. This effect, referred to as truncation by Heffer & Bevan (1990) and Type-C censoring or left-hand truncation by Pickering *et al.* (1995), tends to produce population slopes less steep than their true value, as the effect is proportionally greater for smaller faults.

Fault trace lengths were sampled from the Top Reservoir and Intra-reservoir horizon maps. Many faults continue outside the area of the seismic survey and determining the lengths of the others is also difficult due the large degree of linkage between faults. Only the Top Reservoir example is shown (Fig. 7) as both curves are essentially identical. Fault lengths plot as a gentle convex upwards curve on the cumulative frequency plot. This suggests that the curve suffers from the sampling

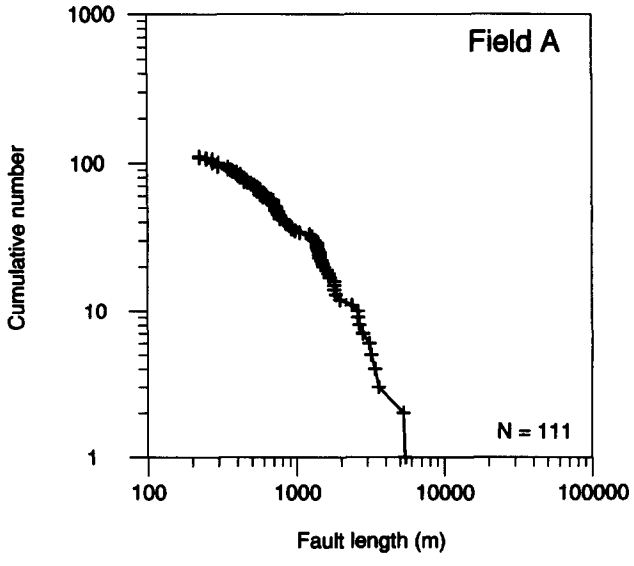


Fig. 7. Observed fault trace lengths for the Top Reservoir horizon, Field A. The upwardly convex nature of the data curve is a result of censoring bias and truncation effects.

effects described above. Short faults are affected by left-hand truncation (Type-C censoring), particularly below lengths of 1000 m. The slope for this data set above a length of 1000 m is −2.04. This lies within the range −1.1 to −2.1, for other fault length data sets that we have analysed (Yielding *et al.* 1996). The curve steepens at the right-hand end (fault lengths over *ca* 3000 m), as faults extend beyond the area of the seismic survey (7 × 12 km). Omitting this part of the data set and calculating a slope for the central part of the data curve gives a value of −1.26 (length range 500–3000 m). However, synthetic tests suggest that it is better to retain those faults that extend outside the data area when calculating slope estimates (Yielding *et al.* 1996). As the size of three-dimensional seismic surveys increases longer faults will be more easily measured. The resolution effect will remain.

### *Fault orientations*

The orientation of seismically-mapped faults was compared with fracture orientation data from core (Fig. 8). The dominant orientation in core is NE–SW although subsidiary WNW–ESE, NW–SE and NNE–SSW trends are also present. The open fractures have two principal trends WNW–ESE and NNW–SSE. Other trends are dominated by fractures which act to reduce reservoir permeability, such as granulation seams and cemented fractures. The open fractures appear to have developed due to the reactivation of existing fractures of types similar to those found in the other orientations. Seismically mapped fault orientations were sampled from the digitized fault polygons (Fig. 8). An azimuth is calculated for each straight line segment of the digitized fault trace. This has the advantage of not being biased against any particular orientation of fault but does produce more azimuth readings where there are more digitized points on the fault trace. Fault tips and intersections are typical examples of such places because fault orientation changes rapidly, requiring more digitized points. This will result in an increased scatter of the measured orientations relative to the 'true' spread of orientations. Both Top Reservoir and Intra-reservoir show strong NE–SW preferred fault orientations. They differ from the core data set in that the subsidiary trends observed in core are not developed. The core data set derives from only one well and it remains to be seen how common these subsidiary trends are in other parts of Field A.

## FAULT POPULATION ANALYSIS, FIELD B

This field is developed in a Middle Jurassic deltaic to marginal marine succession consisting of sands, shales and coals. This sequence was deposited during the thermal subsidence phase following Triassic extension. A full description of the regional tectonics of the northern North Sea, and the Triassic rift event in particular, is given by Roberts *et al.* (1995). Faulting and fracturing

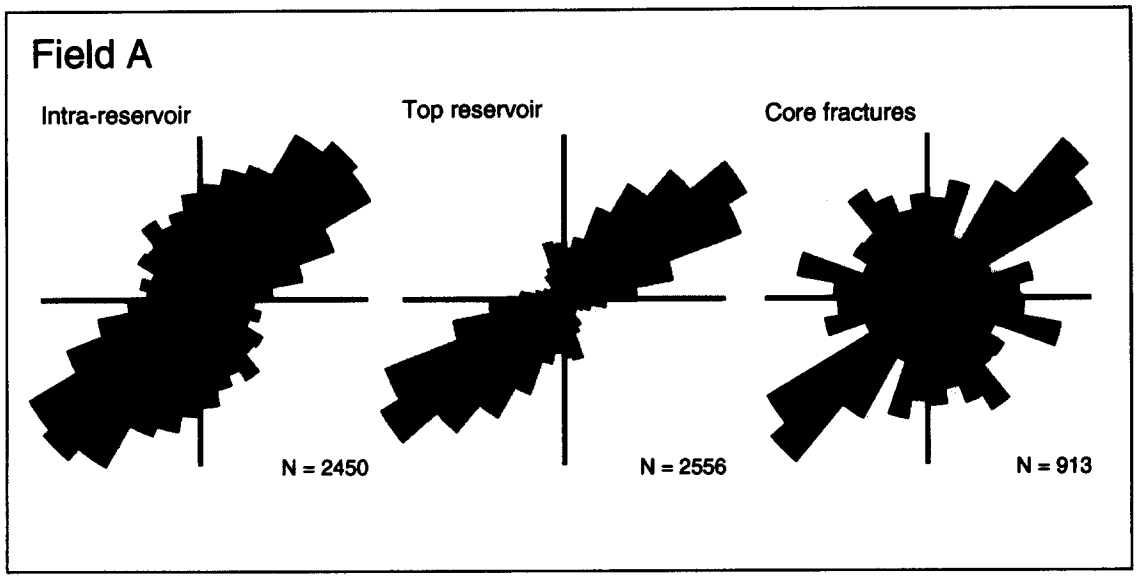


Fig. 8. Fault and fracture azimuths measured from the seismic interpretation and from one well core, from Field A. *N* for the top reservoir and Intra-reservoir horizons refers to the number of fault segments sampled. The core data are samples from a limited area of the field and are strongly influenced by the orientation of local structures.

occurred during Late Jurassic extension. Faulting is absent in core taken from overlying units. Backstripping, using the same techniques as those described by Roberts *et al.* (1995), suggests that the burial depth of the Top Middle Jurassic at the cessation of faulting ranged between 22 and 1947 m. The minimum is an extreme value at the crest of the uplifted and eroded footwall and refers to the top of the studied reservoir unit, which has a present day, compacted, thickness of up to 600 m. Most of the rocks studied in core are likely to have been buried in the range 1500–2500 m during faulting.

Fault population data were extracted from a seismically mapped Intra-reservoir horizon and sub-seismic data obtained from cores from 13 wells. A map of the fault pattern at the Intra-reservoir horizon is shown in Fig. 9. It is particularly important to note that the large N–S fault in the centre of the map is not present in the northern part of the area. Large faults separate the field from a basinal area to the east and a platform area to the west. These are not represented in the data set as they lie outside the area of interest for hydrocarbon production and correlative units are either absent or difficult to identify across the faults. In all 2346 m of core was examined and found to contain *ca* 16,000 fractures. The longest core is 343 m and the shortest is 10.45 m. Except for two well cores, all exceed 100 m in length. In some cases, the entire reservoir section is cored. The dominant, almost exclusive, fracture type is the granulation seam although this shows considerable variation in morphology dependent upon the grain size and clay mineral content of the host rock. Seams tend to be wider and more diffuse in coarser grained, massive sands and more localized in muddier units, with concentrations of aligned clays facilitating slip in the latter. Typical granulation seams show a braided morphology with displacement partitioned between several strands. Displacement values are easily obtained from the fractures

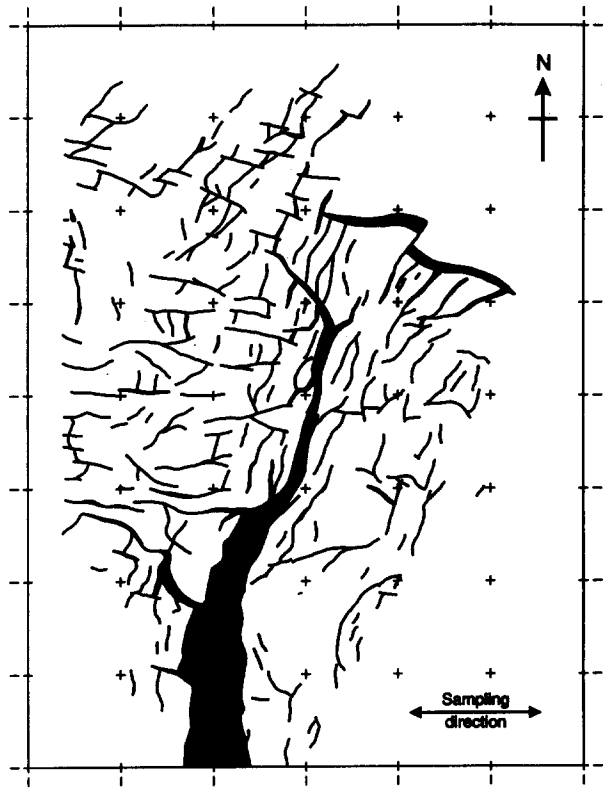


Fig. 9. Map of fault pattern at an Intra-reservoir horizon, Field B. The fault heave polygons are shown in black. A geographic N–S/E–W reference frame is used. Ticks at the grid margin have a 1 km spacing.

in some units as dark coloured organic fragments, such as fossil plant debris, are entrained into the seams and highlight the offset. Some sand bodies are massive however and, although the presence of a granulation seam may be detected, no displacement information can be obtained. Sampling core scale displacements is therefore very lithology-dependent. The Field B fault population was analysed in terms of its displacement, length, spacing and orientation.

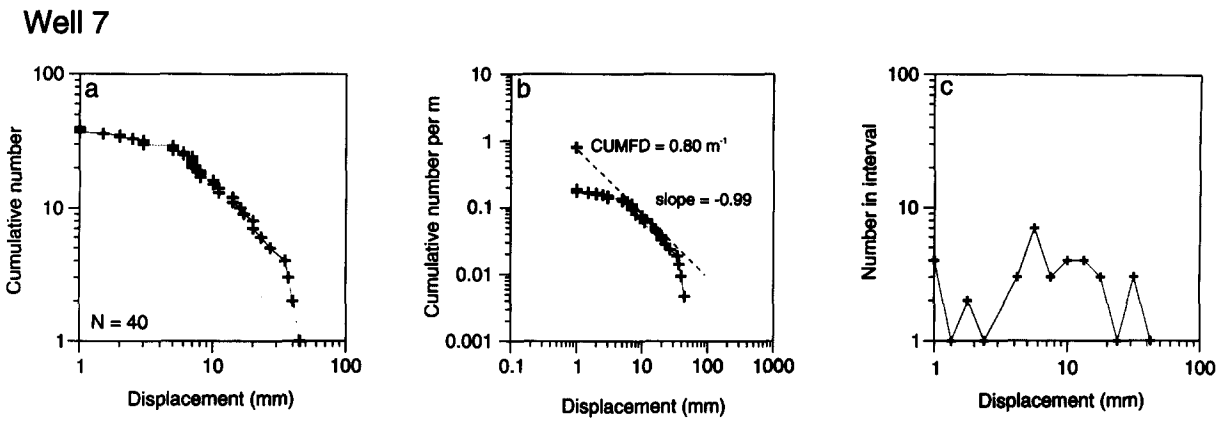


Fig. 10. Fracture displacements from core, Field B well 7. (a) A logarithmic cumulative frequency plot of the data. Note the three-segment form. Undersampling of small displacements occurs due to the limitations imposed by the scale of lithological layering. Large displacements are undersampled owing to the width of the core (10 cm). (b) Plot of the data normalized to cumulative number per m. The entire fault population of the core is expressed as a single point (CUMFD) with a threshold displacement of 1 mm. The projected slope of −0.99 was calculated for the central segment of the displacement curve. (c) Log-interval plot of the same data. Note the irregularity of the curve.

*Core fracture displacements*

All the cores examined contained natural fractures although the cumulative fault density (CUMFD) varies greatly, ranging from 0.36 to 19.31 $m^{-1}$. Two examples of typical well-core displacement cumulative frequency plots are shown in Figs. 10(a) and 11(a). Well 7 has a low CUMFD at 0.80 $m^{-1}$ whilst well 2 has the highest CUMFD value of all the wells at 19.31 $m^{-1}$. Displacement plots from wells often show a characteristic three-segment curve, not unlike a multiline sample, but the causes of the segmentation are slightly different. There is a gently dipping left-hand segment at the low-displacement end of the plot. This is a truncation fall-off effect in that the small displacements are unresolved. This undersampling occurs because of the limitations imposed on recognizing small displacements by the lithological layering in the core. The data curve for well 7 suggests that displacements less than 5 mm are under-represented in the data set. A censoring effect results in the steepening of the curve at the right-hand (high-displacement) end. Not all large displacements can be recognized due to the limitations of the scale of the core. Core slabs are typically 10–12 cm wide, making larger displacements difficult if not impossible to recognize. There is ample evidence that larger displacement faults cut the core. This takes the form of wide deformation zones around slip surfaces and juxtaposition of different lithologies. The omission of only a small number of large displacements results in considerable steepening of the cumulative frequency curve, an effect modelled by Jackson & Sanderson (1992). The lithological effects also have an influence on fractures in the displacement range (1–100 mm) which can be measured in core. Even these may not yield displacement values if bedding is particularly massive. Also, in areas of dense fracturing (e.g. >100 $m^{-1}$), the complexity of the faulting does not allow a measurement to be made of every displacement. Core data cannot therefore be treated in the same way as seismic or outcrop data. It is therefore not amenable to treatment using techniques to correct for censoring due to the omission solely of the largest faults from the data set (Pickering *et al.* 1994).

Well 7 shows a good three-segment curve and it is hoped that the central segment, between displacements of 5 and 30 mm, characterizes the fault population. One way of assessing this is to assume that the cumulative fault density (the total number of fractures divided by

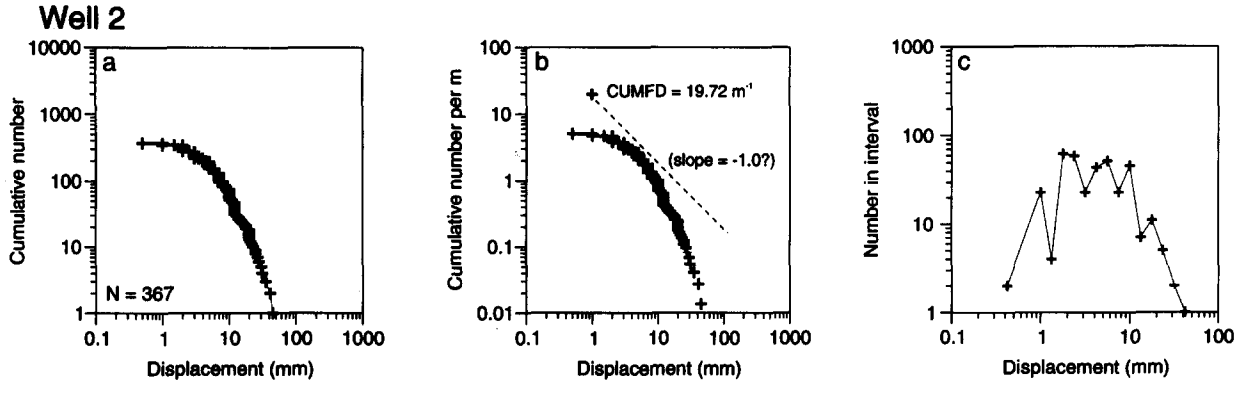


Fig. 11. Fracture displacements from core, Field B well 2. (a) A logarithmic cumulative frequency plot of the data. Note that this curve is strongly influenced by sampling effects with both large and small displacements undersampled. Compare the curve with Fig. 10(a). (b) Plot of the data normalized to cumulative number per m. The entire fault population of the core is expressed as a single point (CUMFD) with a threshold displacement of 1 mm. The projected slope of −1.00 was calculated for the central segment of the displacement curve. Many other slopes could be fitted to this data curve, emphasizing the need for sampling from seismic-scale data in addition to well cores. (c) Log-interval plot of the same data.

the core length) represents the total at some lower threshold value. This value is thought to be about 1 mm, i.e. all fractures recognized in the core have a displacement of at least 1 mm, whether or not that displacement can be measured. The cumulative fault density (CUMFD) value, 0.8 $m^{-1}$, is plotted with the displacement data curve and the slope calculated for the central segment, −0.99 for well 7, is projected to lower values (Fig. 10b). In this case it can be seen that there is a good agreement between the extrapolated slope and the real cumulative fault density data point. The degree to which undersampling (and left-hand truncation) has occurred can also be assessed.

Not all well-core displacement curves show such a good form. Well 2 (Fig. 11) has a high CUMFD and it is difficult to obtain displacement values for all fractures. The curve is severely degraded at the upper and lower displacement ends. This suggests that small and large displacements are undersampled. Plotting the CUMFD value highlights the areas undersampled. Projecting a slope calculated for the central data range shows that the straight line only makes a tangent to the curve. This well data set would be of little value on its own and serves to emphasize that multiple well data sets should be collected and, ideally, compared with seismic-scale displacements.

Slopes calculated for individual wells lie in the range −0.76 to −1.0. Many of the data sets giving steep slopes of −1.0 suffer from the sampling effects described above. Large data sets are not immune from this effect as they are still subject to the limitations of core scale and lithological layering. The data range for core samples covers about two orders of magnitude of displacement. At the lower displacement end 1 mm, or exceptionally 0.5 mm, is the cut-off. The upper limit is usually around 100 mm although the maximum value obtained for all the Field B wells was 240 mm.

The log-interval technique was also applied to Field B core displacements to assess the degree to which data were undersampled. These are presented for well 7 and well 2 in Figs. 10(c) and 11(c), respectively. Both plots are very irregular and it appears that data are not sampled in the central part of the range as well as at the extremes. This is likely due to the limitations imposed by the core described above. Right-hand truncation is marked on the well 2 plot indicating that larger displacements are under-represented in the data. The irregularity of both plots is caused by the variability in the number of data points within adjacent intervals. In addition to the reasons already discussed, the problems of measuring small displacements are also apparent in the plot. Small displacement fractures can, at best, be measured to the nearest 0.5–1 mm. This may appear small, but it is a significant proportion of the size of bin sizes used for this scale in the log-interval technique. Rounding-up rather than rounding-down a displacement value to the nearest millimetre may place it into a different log-interval. Such a variation would be insignificant on outcrop-scale faults with displacements in metres.

*Seismic-scale displacements*

A three-dimensional seismic survey had been acquired over Field B. An Intra-reservoir horizon had been interpreted which had the widest extent of any of the reflectors picked. Interpretation had used both vertical sections and attribute analysis of continuous horizon maps. The latter had allowed subtle, small faults to be interpreted. The horizon grid and fault traces were sampled perpendicular to the dominant fault trend within the field. The multiline displacement sample is shown as a logarithmic cumulative frequency plot in Fig. 12. As with Field A, the three-segment curve is well developed. The left-hand segment indicates that faults with throws of less than 10 m are unresolved, resulting in the gentler slope of the data curve. The sloping segment of the data curve actually continues into the area that should be part of the sampling tail, i.e. below the line on the plot showing the number of sample lines. There is a good geological reason for this. The steep segment represents the multiline sampling of the largest fault in the data set. This fault is not, however, interpreted on all lines as it extends out of the seismic survey area. The largest faults on some of the other lines have much smaller throws and so part of the sampling tail has a much gentler slope. The central segment of the displacement curve, above the sampling tail gives a slope of −0.90. This is calculated for throws in the range 10–50 m.

*Comparison of core and seismic-scale displacements*

The results of the core and seismic-scale one-dimensional displacement sampling are plotted together

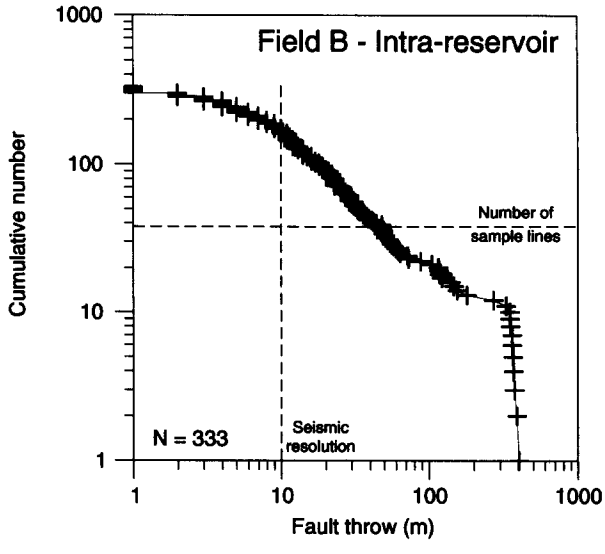


Fig. 12. Logarithmic cumulative frequency plot for multiline one-dimensional sample of fault throws, Intra-reservoir horizon, Field B. The sample comprises fault throws measured on 38 sample lines, total length 156 km. The curve shows the characteristic three-segment form although the moderately-sloping section continues into the sampling tail because the largest fault in the data set does not occur on all lines contributing to the sample (see Fig. 9).

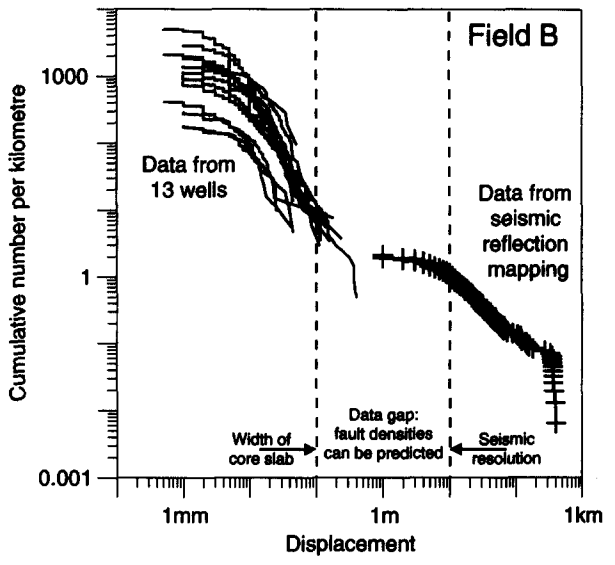


Fig. 13. Comparison of Intra-reservoir seismic-scale throw and well displacement data from Field B. Core-scale displacement data is taken from core from 13 wells.

Table 2. Prediction of sub-seismic fault density for Field B. The second column ('Cumulative fault density') indicates the number of fault cuts greater than or equal to the specified throw per 1 km of horizontal transect. These values are calculated using $N = 8.5d^{-0.90}$ (the best-fit line to the central segment of Fig. 12). The third column ('Fault density per class') indicates the number of fault cuts within each logarithmic class per 1 km of horizontal transect; these values are simply the differences of successive numbers in column 2. For example, the power-law relationship predicts that there are 8.5 fault cuts per km having throw greater than or equal to 1 m, and 7.43 fault cuts per km having throw in the range 1–10 m

| Throw (m) | Cumulative fault density ($km^{-1}$) | Fault density per class ($km^{-1}$) |
|---|---|---|
| 100 | 0.13 | |
| | | 0.94 |
| 10 | 1.07 | |
| | | 7.43 |
| 1 | 8.5 | |
| | | 59 |
| 0.1 | 67.5 | |
| | | 469 |
| 0.01 | 536 | |
| | | 3724 |
| 0.001 | 4260 | |

in Fig. 13. Displacements from all 13 wells are included, normalized to cumulative number per km for comparison with the seismic-scale data. There is a spread of over one order of magnitude which reflects the different fault densities measured in the well cores (0.36–19.31 $m^{-1}$). Extrapolation of a −0.90 slope, that calculated for the seismic data alone, to sub-seismic scales shows that the core data lie on this trend. This suggests that the seismically observed and core-scale-fractures form part of the same population. As with Field A, use of equation (1) allows a prediction of the density of fault cuts of various sizes (throws) to be made. The number of fault cuts in any order-of-magnitude class (e.g. 1–10 m throw) likely to be encountered in a 1 km transect is shown in Table 2 (e.g. 7.43 $km^{-1}$ for fault cuts in the 1–10 m throw range).

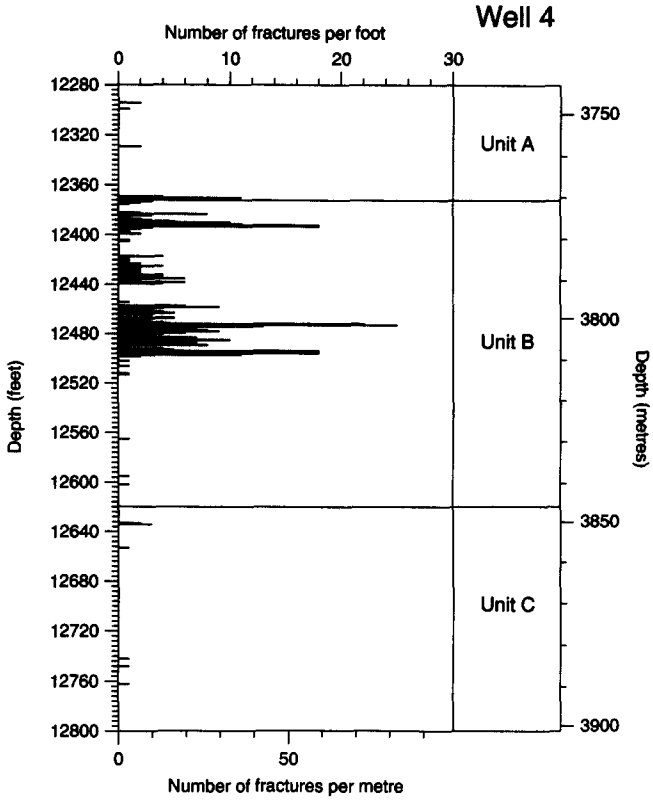


Fig. 14. Fracture distribution in core from well 4, Field B. Fractures are clustered in the upper part of reservoir unit B and are only sparsely developed in units A and C.

### *Core fracture spacing*

It is possible to quantify the fracture spacing and attempt to distinguish the type of spacing distribution that fractures follow. Frequency against depth plots for Field B well cores (Fig. 14) suggest that fractures tend to be clustered rather than having a regular distribution. In the example shown, fractures are concentrated in the upper part of reservoir unit B with densities of up to 25 per foot, i.e. 82.0 $m^{-1}$. Reservoir units A and C have low fracture densities.

Techniques for analysing fracture spacing are described by Gillespie *et al.* (1993) who show that fracture and fault spacing can be treated in a similar manner to displacement. Well cores provide excellent one-dimensional sample lines. Ideally the spacing of fractures could be measured along the core centreline, and spacing plotted as a cumulative frequency diagram. This gives the most direct representation of the spatial distribution of fractures but can be difficult to apply to highly faulted core and large data sets. A less direct technique, but one that is readily applied to long runs of core, is the interval counting method. The analysis is carried out by specifying a number of different interval lengths, e.g. 25 cm, 50 cm, 1 m, etc., or 1 ft, 2 ft, 5 ft, etc. The number $N_i$ of intervals of each size containing at least one fracture is counted. The probability, $p$, of an inverval of length $i$ containing a fracture is given by:

$$p = iN_i/c, \quad (2)$$

where $c$ is the sample line length, i.e. the core length.

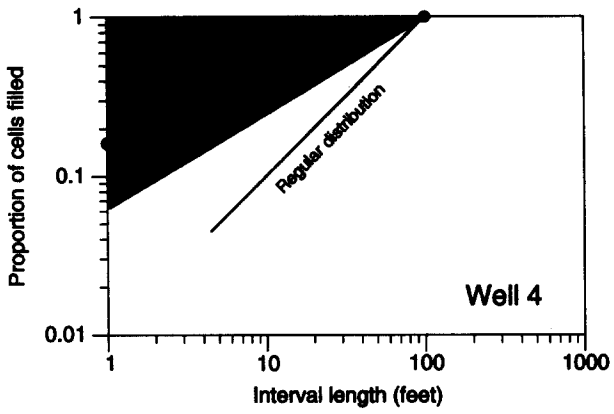


Fig. 15. Interval counting plot of fracture spacing data from well 4, Field B. Data plot as a straight line within the area for fractures with a power-law spacing distribution. The data clearly do not follow a regular spacing distribution.

The proportion of intervals (cells) filled is plotted, on a logarithmic scale, against interval size. The form of the data curve on the plot allows the type of fracture spacing distribution to be determined.

(i) Fractures that have a regular distribution, such as many joint sets, produce a two-segment curve. For interval sizes greater than the maximum spacing the value of $p$ is 1 and the resultant curve has a zero (horizontal) slope. Below the maximum spacing, data plot as a straight line with a slope of 1.0.

(ii) Fractures distributed randomly using a Poisson distribution plot as gentle, upwardly-convex curves with a best-fit slope of 0.82 (Gillespie *et al.* 1993).

(iii) Fractal data sets give lines of constant slope $(1-D_b)$, i.e.:

$$p \propto i^{(1-D_b)} \quad (3)$$

and $0 < D_b < 1$. $D_b$ is a type of fractal dimension termed the box dimension; for ideal fractal distributions it is identical to the fractal dimension (slope) measured on a log–log cumulative frequency plot of fracture spacing. Gillespie *et al.* (1993) concluded that spacing populations of faults frequently have power-law distributions with fractal dimensions ranging from 0.4 to 1.0. This implies that the line of constant slope on the interval counting plot should lie in the range 0–0.6 for fractal data sets, clearly distinguishing them from regular or random distributions. The important characteristic of a fractal spacing distribution is that the fractures are clustered at all scales.

Fracture spacing data from the 13 wells in Field B were analysed using the interval counting technique. Cores were variously depth marked in feet or metres, depending on the age of the core and the operating company. Fracture densities were recorded for every 1 ft or every 25 cm interval as appropriate. The proportion of cells containing at least one fracture was then calculated for intervals which were multiples of the initial interval size. The results for well 4 are shown in Fig. 15. These data plot as a straight line, with a slope of 0.41, which is within the range expected for fractal distributions (Gillespie *et al.* 1993). Applying equation (3) suggests that the fractal (box) dimension controlling fracture spacing in well 4 is 0.59. All the wells give slopes in the range 0.17–0.72. The expected range (for fractal distributions) is 0–0.6: only one of the 13 wells falls outside this range. The observed slopes correspond to fractal (box) dimensions ($D_b$) in the range 0.28–0.83. The core that falls outside the expected range has the lowest CUMFD of all those investigated, at only 0.36 $m^{-1}$. It therefore may not have been sufficiently long to characterize the spacing population adequately.

### *Fault and fracture orientation*

Fault orientations were sampled from the seismic interpretation of the Intra-reservoir horizon (Fig. 16). The azimuth plot shows a symmetrical spread about the dominant NNE–SSW trend. There is also a subsidiary but distinct WNW–ESE trend. The core fracture orientation data show a dominant NNE–SSW to NE–SW trend. Individual well-core fracture sets tend to reflect the dominant orientations of seismically mapped faults adjacent to the well and so some trends may be emphasized more than others, dependent on well location.

## DISCUSSION

The results from Fields A and B indicate that the techniques of fault population analysis can be successfully applied to individual hydrocarbon fields. One-dimensional, line, sampling techniques are particularly well suited to the type of subsurface data, i.e. well cores and seismic lines. Seismic lines, in particular, provide a readily available series of sample lines which, if the survey has been well designed, intersect the main faults at a high angle. The extraction of one-dimensional samples from data held in gridded form is also possible. Two-dimensional, map, samples are more susceptible to sampling effects such as censoring and truncation. Part of this problem will be alleviated as three-dimensional seismic surveys become larger allowing longer faults to be completely sampled. The problem remains that most interpretation effort is concentrated on the crestal areas of structures (i.e. the hydrocarbon-bearing areas). Field-bounding faults and areas 'off-structure' tend not to be interpreted. This introduces a right-hand truncation effect and should be allowed for in the analysis of fault population data from the subsurface. The analyses carried out here suggest that the fault populations in the two fields are controlled by power laws and that the number of intermediate-scale, 1–10 m throw, faults can therefore be predicted.

There have been suggestions (Koestler 1994) that the data gap at the intermediate scale is real and not an artefact of the sampling techniques. Whilst this may be true, there is little in the two data sets presented here to suggest that such a gap exists. The tail-off in seismically observed throws corresponds well with the limit of seismic resolution, and there appears to be no physical reason why an absence of faults of a particular size

should coincide with the resolution limit of the technique used to investigate those faults. Likewise, core-scale investigations indicate the presence of larger faults whose displacements cannot be measured in core but are too small to be imaged seismically. These larger faults appear as clusters of fractures and through-going deformation zones often juxtaposing different lithologies. It is not possible to measure the displacement on these faults in core and although a few may be representative of faults resolvable at the seismic scale most are likely to have displacements below seismic resolution. One possibility for the identification of intermediate-scale faults might be the use of wireline logs from wells in an area for which a detailed stratigraphy exists. This should allow the identification, from vertical separation information in the wells, of faults with a few metres throw.

When analysing a fault population using data collected at different scale of observation, it is important to be certain that the comparison is 'like with like'. In the cases described here it is important to be certain that fractures observed in well core formed contemporaneously with the seismic-scale faults. Also, the faults measured should be from the same unit. The two cases described here are reasonably well constrained. The good correspondence in orientation of seismic- and sub-seismic-scale faults in Field A suggests development as part of the same population. Field B fractures are developed in the Middle Jurassic reservoir succession. This was deposited during post-rift thermal subsidence, following Early Triassic stretching. There was no contemporary faulting. Extension was renewed during the Late Jurassic when the main faults and reservoir-scale fractures formed. In both cases seismic mapping of Top Reservoir or Intra-reservoir faults is being compared with data from core taken from the reservoir interval.

In Field B the dominant fracture type being compared with seismic-scale faults is the shear displacement granulation seam. In Field A the fracture types are more varied. It does appear, however, that other fracture types, such as dilational cemented fractures can also be used in the population analysis. These fractures all accommodate small amounts of deformation, therefore contributing to the sub-seismic component of the total strain (Marrett & Allmendinger 1991, 1992, Walsh *et al.* 1991). At the core scale, fracturing is strongly influenced by the host lithology so that a shear displacement fracture in one bed may have a component of dilation in an adjacent bed and appear as a cemented fracture. Field examples of this behaviour are shown by Peacock & Sanderson (1992).

Analysis of the spacing population suggests that fractures in core follow a power-law distribution, suggesting that there is a degree of clustering of fractures and that they are not regularly distributed. This supports observations of small fractures tending to cluster around larger faults (Jamison & Stearns 1982) separated by relatively unfaulted areas. The variation in cumulative fault densities, greater than one order of magnitude for Field B well cores, also supports the observation of non-uniform fault spacing. With increasing cumulative fault densities, clustering is more difficult to detect as there tends to be more overlap of fault and fracture zones. This gives an overall 'highly fractured' appearance to the core but spacings remain non-regular.

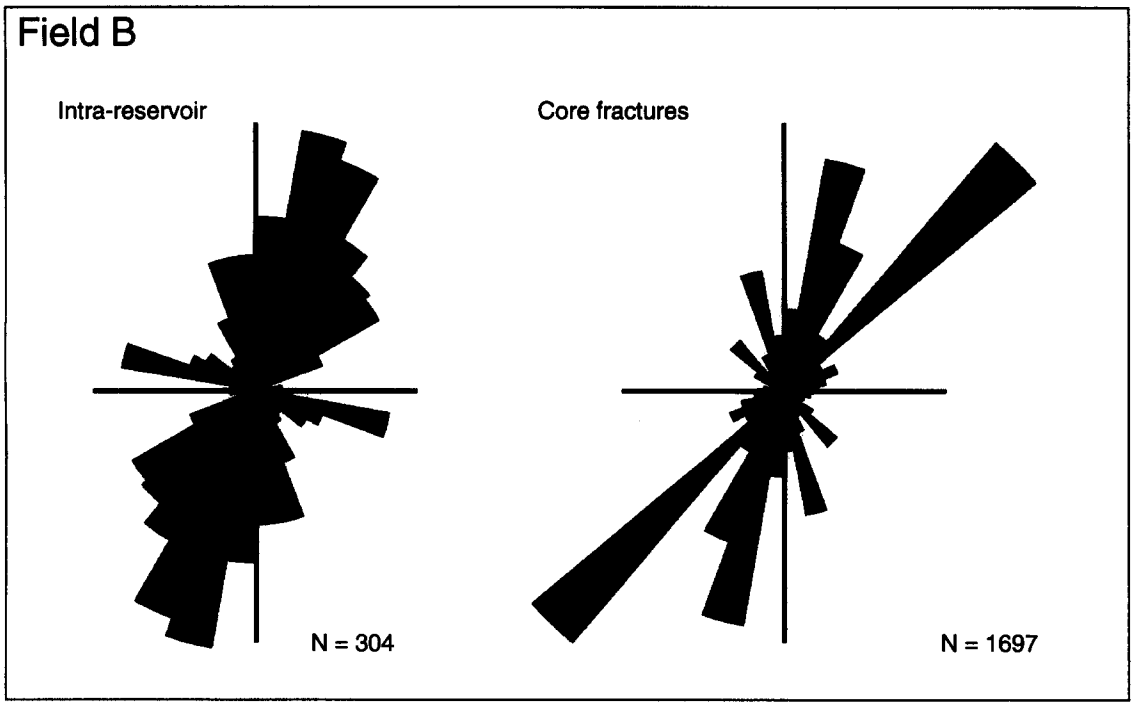


Fig. 16. Fault and fracture azimuths measured from the Intra-reservoir seismic interpretation, and core from 13 wells for Field B. *N* for the Intra-reservoir horizon refers to the number of fault segments sampled. The core data consist of samples from limited areas of the field and are strongly influenced by the orientation of local structures.

## CONCLUSIONS

(1) Sub-surface data is particularly amenable to one-dimensional single- or multiline sampling. Seismic lines, and horizon data in grid form, can be sampled to give multiline one-dimensional descriptions of the fault population. This can be compared with well core data, the core acting as a one-dimensional sample line.

(2) The scale limitations imposed by core can result in data being difficult to sample throughout the scale range (whereas with outcrop and seismic samples the problems are mainly concentrated at the upper and lower resolution limits). The use of a log-interval technique can reveal gaps in the data, but small-displacement fractures that are difficult to measure to better than the nearest millimetre can result in irregularities in the resultant plot.

(3) The data sets presented here suggest that the seismically-resolved faults and core-scale fractures form part of the same continuous population. Any gap in the fault population at intermediate (1–10 m throw) scales would correspond exactly with the resolution limits of the observation techniques (seismic and core). Such a correspondence would be very fortuitous.

(4) Fault length samples (two-dimensional) are more influenced by resolution effects and results are less reliable than one-dimensional samples. The finite size of the sample area (three-dimensional seismic grid) and resolution problems on the distal part of faults are the major controls. The sample areas may be small compared with the length of some structures in the area of interest. This problem will be partly alleviated as three-dimensional seismic surveys become larger. The analysis of fault lengths in areas of linked faults becomes difficult unless detailed fault displacement analysis is performed to determine which splays should be considered part of the same structure. Comparison with regional mapping is also desirable.

(5) Analysis of the spacing of fractures in well cores, using the interval counting technique, suggests that they follow power-law distributions with an exponent in the range $-0.28$ to $-0.83$. The clustered distribution of the fractures clearly distinguishes them from regularly-spaced fracture sets.

(6) For both fields, fault and fracture orientations measured at seismic and sub-seismic scale are similar. Samples taken from individual well cores are strongly influenced by the orientation of the closest seismically-mappable structures and so the position of wells should be considered when analysing the orientation data.

*Acknowledgements*—We thank BP for permission to publish this paper. P. Cowie, G. Pickering and A. Koestler are thanked for their constructive reviews.

## REFERENCES

Antonellini, M. & Aydin, A. 1994. Effect of faulting on fluid flow in porous sandstones: petrophysical properties. *Bull. Am. Ass. Petrol. Geol.* **78**, 355–377.

Childs, C., Walsh, J. J. & Watterson, J. 1990. A method for estimation of the density of fault displacements below the limits of seismic resolution in reservoir formations. In: *North Sea Oil and Gas Reservoirs—II* (edited by Buller, A. T. *et al.*). Graham & Trotman, London, 309–318.

Dalley, R. M., Gevers, E. C. A., Stampfli, G. M., Davies, D. J., Gastaldi, C. N., Ruijtenberg, P. A. & Vermeer, G. J. O. 1989. Dip and azimuth displays for 3D seismic interpretation. *First Break* **7**, 86–95.

Gauthier, B. D. M. & Lake, S. D. 1993. Probabilistic modelling of faults below the limit of seismic resolution in Pelican Field, North Sea, offshore United Kingdom. *Bull. Am. Ass. Petrol. Geol.* **77**, 761–777.

Gillespie, P. A., Howard, C. B., Walsh, J. J. & Watterson, J. 1993. Measurement and characterisation of spatial distributions of fractures. *Tectonophysics* **226**, 113–141.

Heath, A. E., Walsh, J. J. & Watterson, J. 1994. Estimation of the effects of subseismic sealing faults on effective permeabilities in sandstone reservoirs. In: *North Sea Oil and Gas Reservoirs—III* (edited by Aasen, J. Q. *et al.*). Kluwer Academic, 173–183.

Heffer, K. J. & Bevan, T. 1990. Scaling relationships in natural fractures—Data, theory and applications. Reprint No. 20981, 1–12, Society of Petroleum Engineers.

Jackson, P. & Sanderson, D. J. 1992. Scaling of fault displacements from the Badajoz-Cordóba shear zone, SW Spain. *Tectonophysics* **210**, 179–190.

Jamison, W. R. & Stearns, D. W. 1982. Tectonic deformation in the Wingate sandstone, Colorado National Monument. *Bull. Am. Ass. Petrol. Geol.* **66**, 2584–2608.

Koestler, A. G. 1994. Scaling properties of extensional fault populations—the natural gap at the medium scale. Extended abstract. Fault Populations Meeting, Tectonic Studies Group.

Marrett, R. & Allmendinger, R. W. 1991. Estimates of strain due to brittle faulting: sampling of fault populations. *J. Struct. Geol.* **13**, 735–739.

Marrett, R. & Allmendinger, R. W. 1992. Amount of extension on 'small faults': an example from the Viking Graben. *Geology* **20**, 47–50.

Munthe, K. L., Omre, H., Holden, L., Damsleth, E., Heffer, K., Olsen, T. S. & Watterson, J. 1993. Subseismic faults in reservoir description and simulation. Reprint No. 26500, 843–850, Society of Petroleum Engineers.

Peacock, D. C. P. & Sanderson, D. J. 1992. Effects of layering and anisotropy on fault geometry. *J. geol. Soc. Lond.* **149**, 793–802.

Pickering, G., Bull, J. M. & Sanderson, D. J. 1995. Sampling power-law distributions. *Tectonophysics* **248**, 1–20.

Pickering, G., Bull, J. M., Sanderson, D. J. & Harrison, P. 1994. Fractal fault displacements: a case study from the Moray Firth, Scotland. In: *Fractals and Dynamic Systems in Geosciences* (edited by Kruhl, J. H.). Springer, Berlin, 105–119.

Roberts, A. M., Yielding, G., Kusznir, J. J., Walker, I. M. & Dorn-Lopez, D. 1995. Quantitative analysis of extension in the Northern Viking Graben. *J. geol. Soc. Lond.* **152**, 15–26.

Sassi, W., Livera, S. E. & Caline, B. P. R. 1992. Reservoir compartmentation by faults in Cormorant Block IV, U.K. northern North Sea. In: *Structural and Tectonic Modelling and its Application to Petroleum Geology* (edited by Larsen, R. M., Brekke, H., Larsen, B. T. & Talleraas, E.). *Spec. Publ. Norweg. Petrol. Soc.* **1**, 355–364.

Smith, D. A. 1966. Theoretical consideration of sealing and non-sealing faults. *Bull. Am. Ass. Petrol. Geol.* **50**, 363–374.

Walsh, J. J., Watterson, J. & Yielding, G. 1991. The importance of small-scale faulting in regional extension. *Nature* **351**, 391–393.

Walsh, J. J., Watterson, J. & Yielding, G. 1994. Determination and interpretation of fault size populations: procedures and problems. In: *North Sea Oil and Gas Reservoirs—III* (edited by Aasen, J. O. *et al.*). Kluwer Academic, 141–155.

Watts, N. L. 1987. Theoretical aspects of cap-rock and fault seals for single- and two-phase hydrocarbon columns. *Mar. Petrol. Geol.* **4**, 274–307.

Yielding, G., Walsh, J. J. & Watterson, J. 1992. The prediction of small-scale faulting in reservoirs. *First Break* **10**, 449–460.

Yielding, G., Needham, T. & Jones, H. 1996. Sampling of fault populations using sub-surface data: a review. *J. Struct. Geol.* **18**, 135–146.